Effectiveness of oxide trench array as a passive temperature compensation structure in AlN-on-silicon micromechanical resonators

Qingyun Xie, Nan Wang, Chengliang Sun,[a] Andrew B. Randles,[b] Pushpapraj Singh,[c] Xiaolin Zhang, and Yuandong Gu
*Institute of Microelectronics, Agency for Science, Technology and Research (A*STAR), 2 Fusionopolis Way, #08-02, Innovis, Singapore 138634*

(Received 3 December 2016; accepted 5 February 2017; published online 21 February 2017)

This Letter presents the effectiveness of an oxide trench array (OTA) as a passive temperature compensation structure for aluminum nitride on silicon (AlN-on-Si) quasi-surface acoustic wave (SAW) micromechanical resonators over a wide temperature range. Two types of devices, namely, those with OTA and their reference counterparts without OTA, are designed, fabricated, and characterized over a wide temperature range of 360 °C. Experimental results show that the resonator with OTA has a first-order temperature coefficient of frequency (TCf_1) at room temperature (20 °C) of 6.66 ppm/°C, which is lower than that of the reference device without OTA by 72% in magnitude. A high turnover temperature of 197 °C is achieved. Furthermore, the second-order temperature stability of the device has also improved. OTA is experimentally demonstrated to be an effective structure for passive temperature compensation, hence paving the way for using AlN-on-Si resonators as ultrasonic sensors or timing devices in ruggedized environments where the large fluctuation in temperature places stringent demands on temperature stability. *Published by AIP Publishing.*
[http://dx.doi.org/10.1063/1.4976808]

Increasing attention has been paid to piezoelectric acoustic wave microelectromechanical system (MEMS) devices suitable for applications in ruggedized environments such as oil, gas, and aerospace industries.[1–3] The high temperature environment demerits the use of quartz, currently a widely used material in piezoelectric resonators, because it experiences a phase transition at 573 °C, hence adversely affecting the piezoelectric property.[3] Furthermore, quartz resonators, as compared to MEMS resonators, are bulky and not compatible with established complementary metal-oxide semiconductor (CMOS) processes.[4] On the other hand, the deposition of aluminum nitride (AlN), another piezoelectric material, is compatible with established CMOS processes, highlighting the potential of AlN in integrating such ultrasonic devices into CMOS circuits at the chip-level.[5] Another significant merit in AlN lies in its excellent piezoelectric ultrasonic response up to 1150 °C; hence, it is suitable for use in harsh environment applications.[3,6]

The thermal stability of resonance behavior has always been a primary requirement when AlN resonators are used as AlN mechanical, acoustic, and optomechanical resonators, filtering devices, and ruggedized pressure sensors.[5,7–10] This is especially in light of the relatively large temperature coefficient of frequency (TCF) of AlN and Si of approximately −25 ppm/°C and −30 ppm/°C, respectively, which has caused the temperature excursions of resonators made of these materials to be significantly more pronounced than that of quartz crystals.[11–13] Till date, several active and passive temperature compensation methods have been proposed for AlN and Si resonators, in which the latter offers advantages such as eliminating the need for external circuits and reducing power consumption. A popular method is to grow a layer of silicon dioxide (SiO_2) in the resonator structure. SiO_2 has a uniquely positive first-order temperature coefficient of elasticity, which results in a positive TCF of 85 ppm/°C.[1,11,14,15] Further compensating structures such as a matrix of oxide pillars, of various designs, have been demonstrated on silicon resonators, which employ AlN as the active material, for the purpose of temperature compensation of the bulk modes. The bulk oxide compensation techniques have the potential of achieving full temperature compensation of resonance frequency for different resonance modes.[16,17] Other temperature compensation methods reported include varying the propagation direction of quasi-surface acoustic waves (SAWs) and degenerate doping of the resonator structure.[2,18]

This Letter reports on the extension of our previous work[19] by experimentally demonstrating the effectiveness of an oxide trench array (OTA) as a passive temperature compensation structure in AlN-on-Si quasi-SAW micromechanical resonators. Two types of devices, namely, those with OTA and the reference counterparts without OTA, are included. In order to evaluate the effectiveness of OTA as a passive temperature compensation structure, the two types of devices (with and without OTA) are fabricated on the same wafer with the same stack thickness and a similar lateral (*xy*-plane) design. Cross-sectional illustrations of the two types of devices are presented in Fig. 1.

The resonator employs a thin layer of AlN of thickness 1.0 μm as the piezoelectric material. An inter-digitated transducer (IDT) is introduced on top of the piezoelectric layer to excite acoustic waves in the device. In the devices presented in Fig. 1, a sinusoidal voltage is applied to the signal electrodes, labeled as "S," while electrodes labeled as "G" are

[a]Author to whom correspondence should be addressed. Electronic mail: sunc@ime.a-star.edu.sg.
[b]Currently with Invensense Inc., Boston, Massachusetts 02110, USA.
[c]Currently with Centre for Applied Research in Electronics, Indian Institute of Technology Delhi, New Delhi 110016, India.

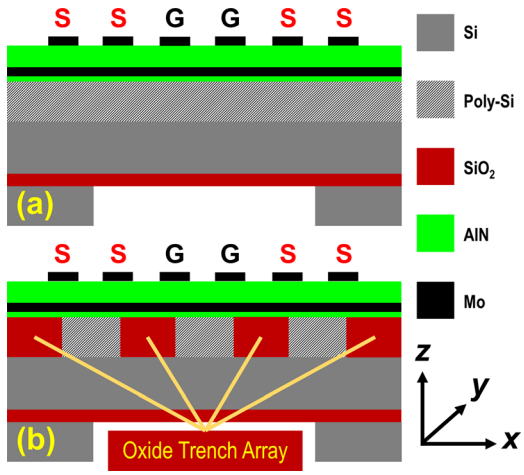

FIG. 1. Illustration of designed devices. (a) Cross-section of the AlN-on-Si resonator without OTA, as the reference design. (b) Cross-section of the designed device with OTA.

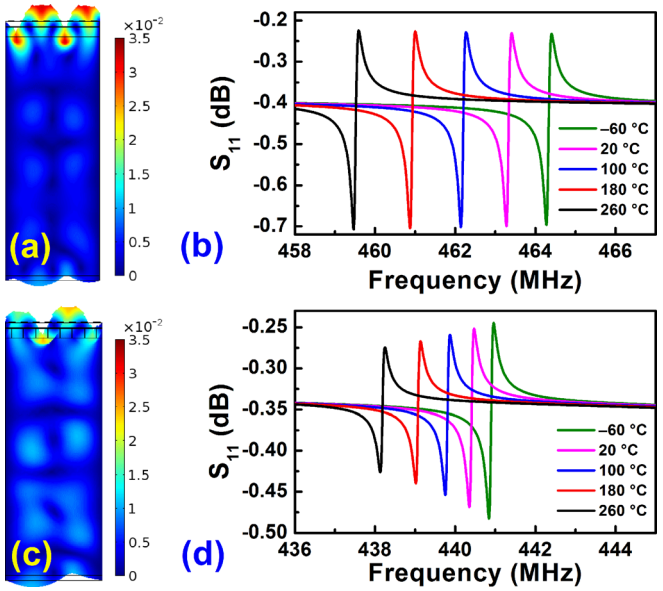

FIG. 2. Results of FEM simulation: (a) Quasi-SAW mode shape supported by the device without OTA; (b) shift in the S_{11} spectrum of the mode in (a) over a range of temperatures; (c) quasi-SAW mode shape supported by the device with OTA; and (d) shift in the S_{11} spectrum of the mode in (c) over a range of temperatures.

grounded. A layer of molybdenum (Mo) is introduced between the AlN and poly-Si/OTA layers to create a strong time-harmonic electric field between this metallized surface and the IDT.

An oxide trench array, a passive temperature compensation feature, is introduced in the layer of poly-crystalline silicon (poly-Si) of the same thickness, as presented in Fig. 1(b). Each oxide trench is exactly centered between the adjacent signal and ground electrodes. These positions on the surface of the resonator and along the x-axis correspond to the regions of maximum strain, which results in the most effective passive compensation, because the contribution to strain by thermal effects will be reduced.[17] The OTA extends in the y-direction to match the overlapping length of the signal and ground electrodes. The geometry of the OTA, including the width and height of each trench, was carefully designed using a methodology reported in our previous work,[19] in order to ensure effective temperature compensation over a wide range of temperature while achieving the desired resonance frequency.

Finite element method (FEM) simulations were performed using COMSOL Multiphysics to investigate the RF performance of our proposed design. In 2D simulations of the frequency response, one pair of fingers was used with periodic boundaries in the left and right sides of the device. The periodicity of the IDT was designed to be 10.36 μm and 9.22 μm for the devices without and with OTA, respectively. The split IDT design was employed. Each oxide trench is designed to be of width 2.4 μm. The height of the silicon device layer, buried oxide (BOX), and poly-Si/OTA layers are 50 μm, 1 μm, and 2 μm, respectively.

Figs. 2(a) and 2(c) illustrate the quasi-SAW mode shape supported by each type of device at the room temperature (T_{rm}) of 20 °C. The resonance frequencies of the devices without and with OTA are 463.28 MHz and 440.35 MHz, respectively. The phase velocities of the fundamental mode of the quasi-SAW are deduced as approximately 4800 m/s and 4060 m/s, respectively. The main cause of reduction in phase velocity (by 15%) is attributed to the addition of substantial amounts of silicon dioxide into the composite structure. In particular, from the simulation mode shapes reported in Fig. 2(c), it is observed that the acoustic wave induces significant displacement in the OTA regions, possibly indicating the effect of oxide in the reduction of phase velocity of quasi-SAW. The flexibility of this design provides an option to tune the spacing between the IDTs to obtain desired resonance frequencies for a particular mode, hence allowing this resonator design to be customized for a wide range of frequencies.

The temperature dependence of the resonance profile was investigated by introducing temperature-dependent material properties into each of the two device models. Figs. 2(b) and 2(d) present the shift in S_{11} over the same temperature range for the devices without and with OTA, respectively. For a similar quasi-SAW mode, the resonance frequency of the device with OTA experiences a significantly smaller magnitude shift as compared to the resonance frequency of the device without OTA. The aforementioned simulations support that OTA improves the temperature stability of the resonance frequency of the designed devices.

Two types of devices, namely, those with OTA and their reference counterparts without OTA, were fabricated based on our in-house AlN-on-Si platform. The fabricated devices are designed to have the same dimensions as those of the simulation model. The CMOS-compatible process flow begins with an 8-inch silicon-on-insulator (SOI) wafer with a device layer of 50 μm and a buried oxide (BOX) layer of 1 μm. First, a layer of thermal oxide of thickness 2 μm is grown and patterned. All regions other than regions of OTA are etched and are filled with poly-Si. Chemical-mechanical polishing (CMP) is performed to ensure a uniform thickness of OTA and poly-Si. Next, layers of AlN (seed layer), bottom Mo, AlN, and top Mo of thicknesses 20 nm, 0.2 μm, 1.0 μm and 0.2 μm, respectively, are deposited successively. In order to obtain the IDT, the top Mo is patterned. Lastly, a backside etch is performed to release the structure. Images of

the fabricated devices, taken using a scanning electron microscope (SEM), are presented in Fig. 3.

In order to quantify the sensitivity of the device resonance frequency against temperature T, the following Taylor polynomial is used:[14,16]

$$f(T) = f(T_0)\sum_{n=0}^{N} \mathrm{TC}f_n(T_0) \times (T - T_0)^n, \tag{1}$$

where T_0 is an arbitrary reference temperature. The limit $N \to \infty$ may be used to theoretically include all higher-order terms of T. It follows from (1) that $\mathrm{TC}f_n(T_0)$, the n-th order temperature coefficient of frequency at T_0, may be evaluated as

$$\mathrm{TC}f_n(T_0) = \left\{\frac{1}{n!f(T)}\frac{\partial^n f(T)}{\partial T^n}\right\}\Bigg|_{T=T_0} \tag{2}$$

with units of $1/^\circ\mathrm{C}^n$.

The temperature coefficients of frequency of the fabricated devices were investigated to evaluate the effectiveness of our proposed design for temperature compensation. The devices were characterized over a wide temperature range of 360 °C (−60 °C to 300 °C) using a Cascade Microtech vacuum probe station. The frequency response of the device at each operating temperature was measured using a network analyzer (Agilent E5071B), which is calibrated by the Short-Open-Load-Through (SOLT) method. In order to ensure a relatively uniform temperature throughout the structure of the device, the final microwave readings were only extracted after significant time of stabilization. Fig. 4 presents the S_{11} output of the devices at various operating temperatures for both resonators with and without OTA.

The fractional shift in the resonance frequency of the resonator, here defined as $\Delta f(T)/f(T_{\mathrm{rm}})$, where $\Delta f(T) = f(T) - f(T_{\mathrm{rm}})$, is presented in Fig. 5(a). In this work, the second-order version of (1), where $N = 2$, is used as the regression model. It is evident from Figs. 4(b) and 5(a) that the introduction of OTA into the resonator has significantly

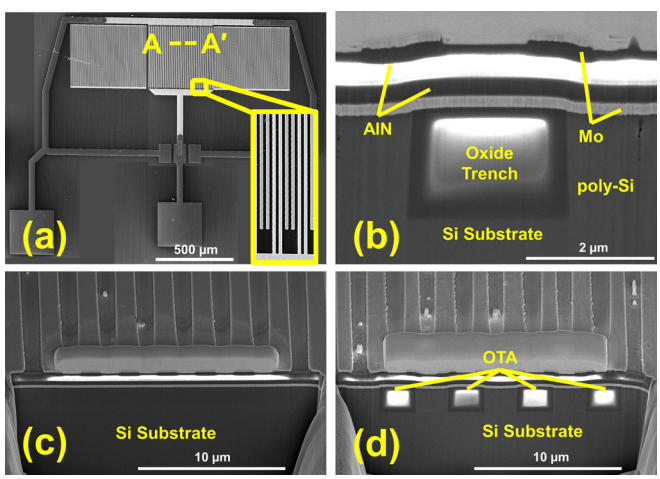

FIG. 3. SEM images of fabricated devices. (a) Top view of a device, with a close-up view of the IDT included as an inset; (b) Cross-section A–A′, illustrating one oxide trench; (c) Cross-section A–A′ of the device without OTA; (d) Cross-section A–A′ of the device with OTA. The materials are labeled on the images.

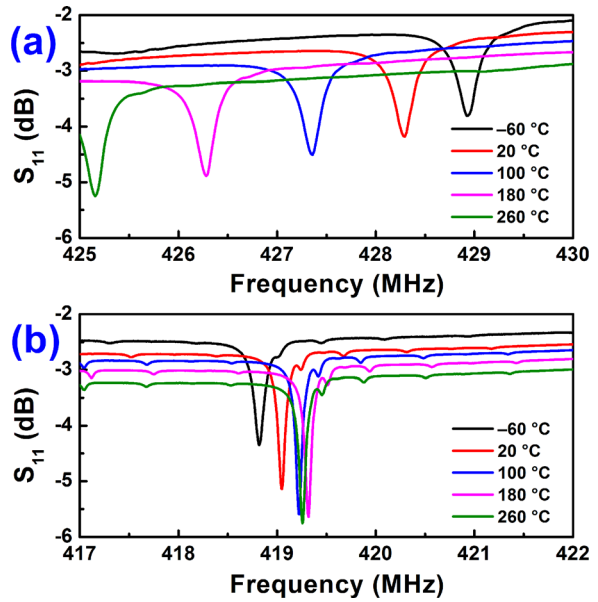

FIG. 4. Device S_{11} measurements over various operating temperatures, for devices (a) without OTA and (b) with OTA.

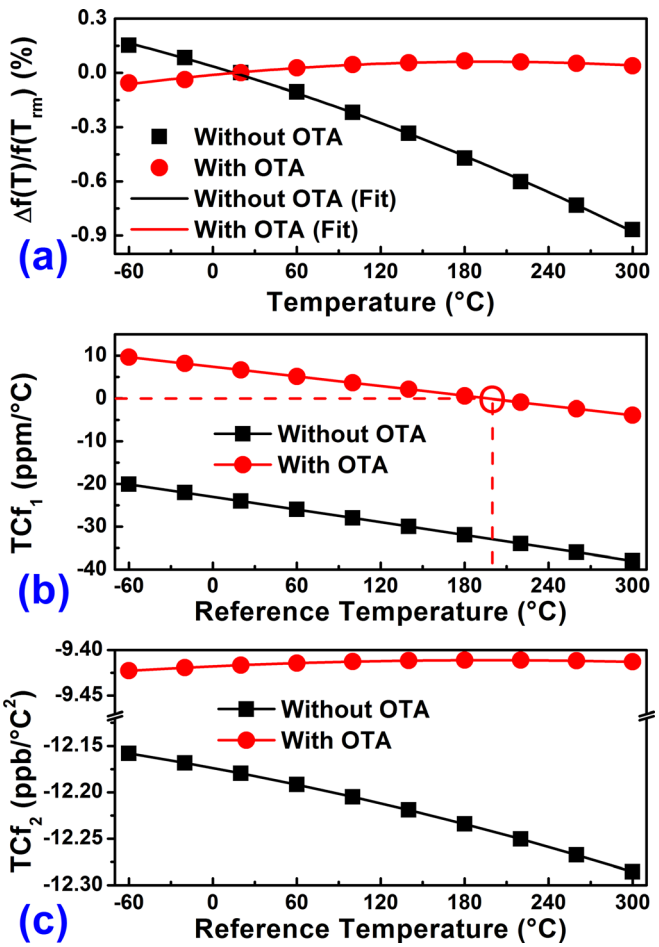

FIG. 5. Summary of extracted TCF results. (a) Comparison of fractional resonance frequency variation between the devices with and without OTA. A second-order best-fit line according to (1) ($N = 2$) is drawn. (b) Plot of $\mathrm{TC}f_1$ of both devices as a function of the reference temperature T_0. The location of turnover temperature is indicated as a hollow bullet. Note that TOT is in range only for the device with OTA. (c) Plot of $\mathrm{TC}f_2$ of both devices as a function of the reference temperature T_0.

TABLE I. A comparison of temperature-dependent characteristics of devices with and without OTA.

Parameter	Without OTA	With OTA
$TCf_1(T_{rm})$ (ppm/°C)	−24.00	6.66
$TCf_2(T_{rm})$ (ppb/°C^2)	−12.18	−9.42
Turnover Temp. (°C)	N.A.	197
TCf_2(TOT) (ppb/°C^2)	N.A.	−9.41

reduced the fractional shift in the resonance frequency, therefore improving the temperature stability of the resonator performance. The phase velocity of quasi-SAW decreased by 13% after the addition of OTA. This is a similar result as predicted by simulations.

Table I summarizes the temperature parameters of the devices with and without OTA. Notably, the introduction of OTA has decreased the TCf_1 by 72% in magnitude (from −24.00 ppm/°C to 6.66 ppm/°C) at room temperature. The variation of the TCf_1 against reference temperature is presented in Fig. 5(b). The TCf_1 of the resonators with OTA is significantly lower in magnitude than that of the resonators without OTA, across the entire wide range of temperatures measured. This indicates the effectiveness of such structures as a passive temperature compensation structure for AlN-on-Si micromachined resonators over a wide temperature range of 360 °C. The turnover temperature, which is inferred from the condition $TCf_1 = 0$, is 197 °C. The high turnover temperature makes this resonator most suitable for deployment at such an operating point.

The effectiveness of our designed OTA is also reflected in the smaller magnitude and higher stability of the resonator's TCf_2 over the wide measured range of temperatures, as presented in Fig. 5(c). TCf_2 at room temperature has been reduced in magnitude from −12.18 ppb/°C^2 to −9.42 ppb/°C^2, while TCf_2 at turnover temperature is −9.41 ppb/°C^2. All of the above-mentioned temperature coefficients reveal that OTA has significantly reduced the temperature variation of the device resonance behavior.

In summary, OTA is verified to be an effective passive temperature compensation structure in AlN-on-Si resonators using a combination of simulation and characterization of fabricated devices. The design is experimentally proven to significantly reduce the TCf_1 by 72% in magnitude to 6.66 ppm/°C. The above-mentioned temperature coefficients reveal that OTA has significantly reduced the temperature variation of the device resonance behavior over a wide temperature range of 360 °C. A high turnover temperature of 197 °C is achieved in order to deploy this resonator in harsh environments. This temperature compensated resonator exhibits a huge potential as an ultrasonic sensor (e.g., pressure sensor) in ruggedized environments with wide temperature fluctuations, thanks to the excellent thermal stability of the resonator with an oxide trench array.

The authors gratefully acknowledge Dr. Yao Zhu for the invaluable discussions. This work was supported by the Science and Engineering Research Council of Agency for Science, Technology and Research (A*STAR), Singapore, under Grant No. 1421500072.

[1]C.-M. Lin, T.-T. Yen, V. V. Felmetsger, M. A. Hopcroft, J. H. Kuypers, and A. P. Pisano, Appl. Phys. Lett. **97**, 083501 (2010).
[2]P. M. Davulis and M. P. D. Cunha, IEEE Trans. Ultrason. Ferroelectr. Freq. Control **57**, 59 (2010).
[3]R. Turner, P. Fuierer, R. Newnham, and T. Shrout, Appl. Acoust. **41**, 299 (1994).
[4]M. Rinaldi, C. Zuo, J. V. der Spiegel, and G. Piazza, IEEE Trans. Electron Devices **58**, 1281 (2011).
[5]Y. Zhu, N. Wang, C. Sun, S. Merugu, N. Singh, and Y. Gu, IEEE Electron Device Lett. **37**, 1344 (2016).
[6]N. Patel and P. Nicholson, NDT Int. **23**, 262 (1990).
[7]G. Wu, Y. Zhu, S. Merugu, N. Wang, C. Sun, and Y. Gu, Appl. Phys. Lett. **109**, 013506 (2016).
[8]N. Wang, F.-L. Hsiao, M. Palaniapan, and C. Lee, Appl. Phys. Lett. **99**, 234102 (2011).
[9]S. Ghosh and G. Piazza, Opt. Express **23**, 15477 (2015).
[10]X. Mu, P. Kropelnicki, Y. Wang, A. B. Randles, K. T. C. Chai, H. Cai, and Y. D. Gu, Appl. Phys. Lett. **105**, 113507 (2014).
[11]G. Wingqvist, L. Arapan, V. Yantchev, and I. Katardjiev, J. Micromech. Microeng. **19**, 035018 (2009).
[12]J. L. Fu, R. Tabrizian, and F. Ayazi, IEEE Trans. Electron Devices **61**, 591 (2014).
[13]W.-T. Hsu and C. T.-C. Nguyen, in *Technical Digest of the 15th IEEE International Conference on Microelectromechanical Systems* (2002), pp. 731–734.
[14]R. Melamud, B. Kim, S. A. Chandorkar, M. A. Hopcroft, M. Agarwal, C. M. Jha, and T. W. Kenny, Appl. Phys. Lett. **90**, 244107 (2007).
[15]J. Zou, C.-M. Lin, Y.-Y. Chen, and A. P. Pisano, J. Appl. Phys. **115**, 094510 (2014).
[16]R. Tabrizian, G. Casinovi, and F. Ayazi, IEEE Trans. Electron Devices **60**, 2656 (2013).
[17]V. A. Thakar, Z. Wu, A. Peczalski, and M. Rais-Zadeh, J. Microelectromech. Syst. **22**, 815 (2013).
[18]A. K. Samarao and F. Ayazi, IEEE Trans. Electron Devices **59**, 87 (2012).
[19]A. B. Randles, J. M. Tsai, P. Kropelnicki, and H. Cai, J. Autom. Control Eng. **2**, 191 (2014).